Copyright WILEY-VCH Verlag GmbH & Co. KGaA, 69469 Weinheim, Germany, 2013.

ADVANCED MATERIALS

Supporting Information

for *Adv. Mater.*, DOI: 10.1002/adma.201203483

Electron Doping by Charge Transfer at $LaFeO_3/Sm_2CuO_4$ Epitaxial Interfaces

Flavio Y. Bruno, Rainer Schmidt, Maria Varela, Javier Garcia-Barriocanal, Alberto Rivera-Calzada, Fabian A. Cuellar, Carlos Leon, Pardeep Thakur, Julio C. Cezar, Nicholas B. Brookes, Mar Garcia-Hernandez, Elbio Dagotto, Stephen J. Pennycook, and Jacobo Santamaria**

Supporting Information

Electron Doping by Charge Transfer at $LaFeO_3/Sm_2CuO_4$ Epitaxial Interfaces

By *Flavio Y. Bruno***, *Rainer Schmidt*, *Maria Varela*, *Javier Garcia-Barriocanal*, *Alberto Rivera-Calzada*, *Fabian A. Cuellar*, *Carlos Leon*, *Pardeep Thakur*, *Julio C. Cezar*, *Nicholas B. Brooks*, *Mar Garcia-Hernandez*, *Elbio Dagotto*, *Stephen J. Pennycook* and *Jacobo Santamaria***

Dr. F.Y. Bruno*, Dr. R. Schmidt, Dr. M. Varela, Dr J. Garcia-Barriocanal, Dr. A. Rivera-Calzada, Dr. F.A. Cuellar Dr. C. Leon, Prof. J. Santamaria*
GFMC. Dpto. Física Aplicada III, Universidad Complutense de Madrid, Campus Moncloa, Madrid, 28040 (Spain)
E-mail: flavioyb@fis.ucm.es, jacsan@fis.ucm.es

Dr. M. Varela, Dr. E. Dagotto, Dr. S.J. Pennycook
Materials Science and Technology Division, Oak Ridge National Laboratory, Oak Ridge, Tennessee 37831-6071 (USA)

Dr. P. Thakur, Dr. J.C. Cezar, Dr. N.B. Brooks
European Synchrotron Radiation Facility (ESRF), 6 rue Jules Horowitz, B.P. 220, Grenoble Cedex 38043 (France)

Dr. Mar Garcia-Hernandez
Instituto de Ciencia de Materiales de Madrid, Consejo Superior de Investigaciones Cientificas, Cantoblanco 28049 (Spain)

Dr. E. Dagotto
Department of Physics and Astronomy, University of Tennessee, Knoxville, Tennessee 37996 (USA)

Band alignment

In this section we provide an estimation of the band alignment of $LaFeO_3$ (LFO) and Sm_2CuO_4 (SCO) following the method described by *Yunoki et al.* [1] The band alignment of these Mott insulators with respect to Nb:$SrTiO_3$ is used to obtain the relative chemical potential position between them. This method is consistent with the determination of work functions by x-ray photoemission spectroscopy (XPS) [2]. In figure SI1 we show the upper (UHB) and lower Hubbard band (LHB) for LFO and SCO, as well as the charge transfer band (CTB). Note that in both materials the energy difference (Δ) between CTB and UHB is smaller than the energy difference between the UHB and the LHB (U), i.e. the gap in both of these materials is of the charge-transfer (CT) type. The schematic band diagram of SCO is taken from ref [2]. The values of Δ and U for LaFeO3 are taken from ref [3] and the

chemical potential is assumed to be in the middle of the charge transfer gap. According to this band diagram the chemical potential of LFO is 0.86 eV above the chemical potential of SCO.

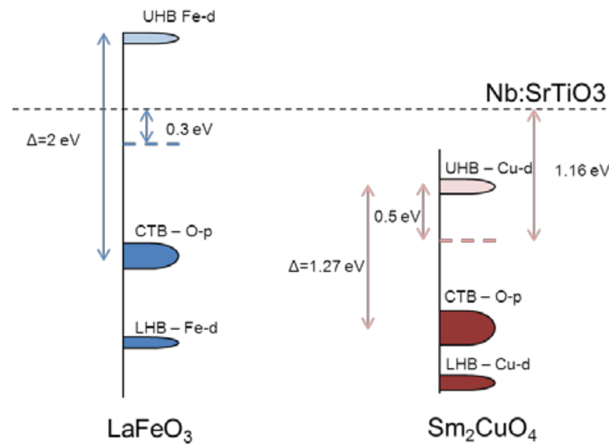

Figure SI1. Schematic band structure for p (charge transfer band - CTB) and d states (upper and lower Hubbard band) lineup of $LaFeO_3$ (blue) and Sm_2CuO_4 (brown) aligned relative to the Fermi level of Nb:$SrTiO_3$. The broken lines are the Fermi levels, dark (light) bands are full (empty).

X-ray diffraction

Structural characterization using x-ray diffraction was performed in a four-circle Philips X´pert-PRO MRD diffractometer with Cu cathode (wavelength λ=0.15418 nm). Selected samples were characterized using synchrotron radiation of wavelength λ=0.08186 nm at the beam line BM25B of the European Radiation Synchrotron Facility (ESRF). Figure SI2a and b show x ray reflectivity and diffraction spectra respectively for a superlattice $[LFO_{14}/SCO_2]_6$. In the reflectivity spectra clear superlattice peaks and finite size oscillations are observed. In the diffraction spectra many narrow superlattice peaks are observed proving the high quality and low roughness of the interfaces between LFO and SCO. Due to the small (2u.c.) SCO thickness in this superlattice the broadening of the Bragg peak as well as the overlapping superlattice Bragg peaks make impossible to locate its position accurately enough to calculate the lattice parameters. X-ray diffraction of a 6 u.c. thin film grown in the same conditions shows that the lattice parameter is c=1.196 nm corresponding to a pure T´structure.

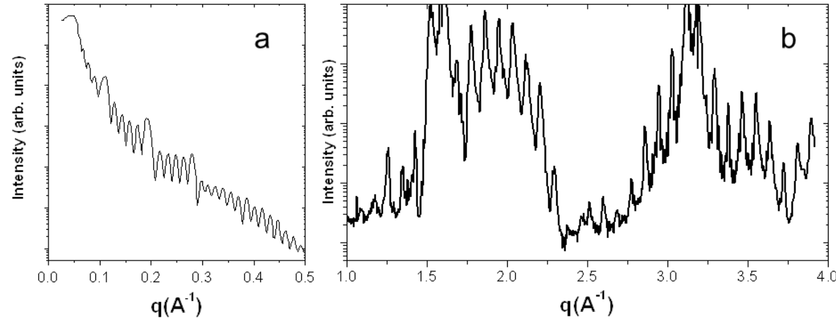

Figure SI2. (a) X-ray reflectivity and (b) x-ray diffraction spectra of a $[LFO_{14}/SCO_2]_6$ heterostructure.

To further investigate the structural characteristics of our heterostructures we measured X-ray reciprocal space maps. For simplicity we label points in the reciprocal space Q = (q_x,q_y,q_z) with coordinates (H,K,L) = (q_x a/2π, q_y a/2π, q_z a/2π) in reciprocal lattice units where a is the lattice parameter of the STO substrate. We studied (H,K,L) points in the reciprocal space with semi-integer values of H,K and L where no intensity from the substrate is detected, however, because LFO is tetragonally distorted we are able to obtain its lattice parameters by studying these points. We measured reciprocal space maps around the (0.5 0.5 1.5) sites. Figure SI3a displays clearly visible superlattice peaks. The maximum intensity is located at (0.5 0.5 1.479) and the intensity profile is elongated along the L direction corresponding to the finite thickness of the film along the growth direction. Figure SI3b shows the reciprocal space map associated with in plane lattice parameters. The maximum intensity is located at H = K = 0.5, proving that the LFO grows with the lattice parameters matching those of the STO substrate. The lattice parameters of the LFO can be calculated yielding a = (0.391+/-0.001) nm and c = (0.396+/-0.001) nm corresponding to a shortening of the in plane lattice parameters to match those of the substrate. To obtain lattice parameters of the SCO we studied the reciprocal space point (0 1 2.2). We can work out the in plane lattice parameters of the SCO from Figure SI3d obtaining a = b = (0.391+/-0.001) nm, but it is not possible to calculate the out of plane lattice parameter due to the broadening of the peak in the

L direction (Fig. SI3c). Thus both LFO and SCO are fully strained and have the lattice parameters of the STO in the plane of the substrate.

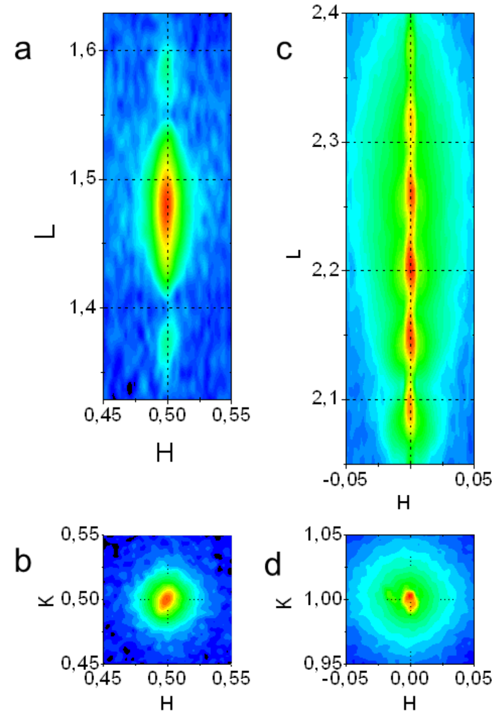

Figure SI3. Reciprocal space maps of $[LFO_{14}/SCO_2]_6$ heterostructure: (a) and (b) are taken around (0.5 0.5 1.5) (c) and (d) are taken around (0 1 2.2) reciprocal lattice points.

Scanning Transmission Electron Microscopy

Figure SI4 displays an atomic resolution high angle annular dark field (ADF) scanning transmission electron microscopy image (also known as Z-contrast) of a $[LFO_{14}/SCO_4]_6$ superlattice. This image corresponds to the area where the elemental maps have been acquired (see Figure 1d main text). In the Figure SI4 the atomic planes are indicated by color bars. The chemical information is obtained from the elemental maps (see main text Figures 1e-i).

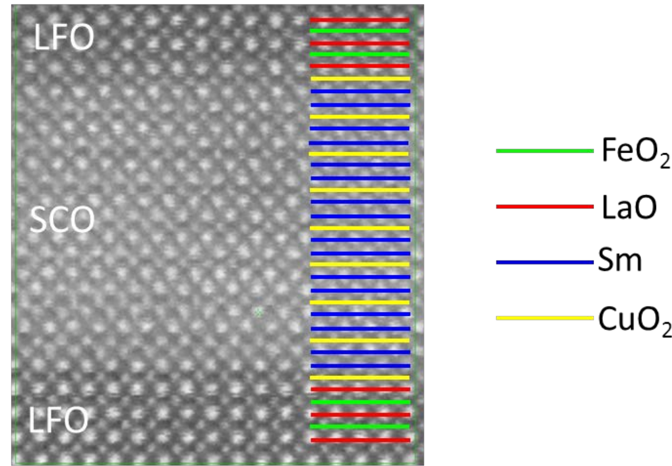

Figure SI4. High-resolution scanning transmission electron microscopy image of a $[LFO_{14}/SCO_4]_6$ heterostructure. The atomic planes are indicated by color bars: FeO_2 (green), LaO (red), Sm (blue) and CuO_2 (yellow).

Impedance Spectroscopy

The constant-phase element (CPE) behavior is usually explained by a broadening of the distribution of relaxation times τ across the macroscopic sample, where $\tau = R \cdot C$, with R being the resistance and C the capacitance of an ideal RC element. The impedance Z_{CPE}* of a CPE is defined as:

$$Z^*_{CPE} = \frac{1}{C_{CPE}(i\omega)^n}\ ; \qquad (1)$$

where C_{CPE} is the CPE specific capacitance, which can be converted into a real capacitance [1], ω is the angular frequency and n the critical exponent with typical values of $n = 0.6 - 1$. $n = 1$ constitutes the ideal case of an ideal capacitor. In an R-CPE circuit, decreasing n values indicate a broadening of the distribution of τ. The exact shape of the distribution of τ is not accessible from impedance spectroscopy data, and the exponent n constitutes a semi-empirical parameter to reflect increasing width of the distribution of τ by decreasing n values.

The intrinsic film contribution of the LFO control sample exhibits an activation energy of 0.13 eV, whereas the SCO control sample exhibits 0.26 eV.

The assignment of the 3 dielectric relaxations to one electrode/sample surface and two LFO/SCO interface contributions was confirmed by the temperature dependence of the capacitors associated with each relaxation (Fig 4d). The CPE capacitance obtained from the fits was always converted into a real capacitance C. The LFO/SCO interface capacitor C1 displays a low capacitance, which has the temperature dependence typical for STO. This indicates that the resistor R1 was measured in-plane and in parallel with the substrate since in-plane capacitive contributions are always expected to be low due to the small in-plane current cross section *A*. Therefore, we associate R1-CPE1 with one low resistance LFO/SCO interface and one parallel capacitance STO substrate contribution (see also the electric field lines in the upper inset of Figure 4b).

On the other hand, out-of plane capacitive contributions are expected to be high due to relatively large *A* in comparison with the microscopic film thickness *d*. Capacitors C2 and C3 both display high capacitance and may be, therefore, associated with out-of-plane contributions. This is expected for the electrode / film surface interface contribution (R3-CPE3) and R3 may well represent the contact resistance, which is eliminated and, thus, not visible by Van der Pauw measurements. The origin of the out-of-plane LFO/SCO interface contribution R2-CPE2 is less clear. Possibly, it represents a LFO/SCO interface contribution in sample areas close to the electrodes, i.e. directly below. This may be supported by the notion that the electric field lines near such sample areas below the electrodes are passing mainly perpendicular across the LFO/SCO interface (out-of-plane), whereas the electric field lines between the electrodes are mainly in parallel with the interface (in-plane) (see Figure 4b upper inset). The in-plane capacitance values for the LFO_{21} and SCO_5 control samples grown on identical STO substrates align well with C1 (Fig. 4d), which may further support the notion that C1 is a substrate contribution.

All dielectric measurements described above were also carried out under fixed applied magnetic fields between 0.05 – 10 Tesla, but none of the 3 dielectric relaxations detected showed any significant magneto-resistance or magneto-capacitance at any temperature.

DC transport

To further inspect the transport properties of the superlattices we measured the resistance of $[LFO_{14}/SCO_4]_6$ at different current levels. In Figure SI5 we show successive resistivity measurements on this sample. The upward jump in the resistance occurs at the point where is

not longer possible to inject a current. The measured resistance values are the same for different current levels what demonstrates the reliability of the measurement and the absence of electro-resistance. Several attempts have been made to improve the quality of the contacts to the sample however these were unsuccessful. Resistance measurements on Figure 4a were made using evaporated silver spots, measurements in Figure SI5 were made after wire bonding with Al, a method that proved to be useful in contacting conducting interfaces of other materials. Finally, buried contacts through ion beam etching and filling with Ti also displayed high contact resistance.

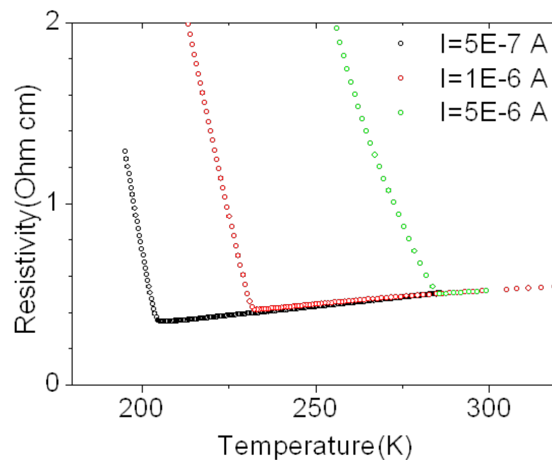

Figure SI5: Resistivity as a function of temperature of a $[LFO_{14}/SCO_4]_6$ heterostructure. The measurements where done applying different currents.

References

[1] S. Yunoki, A. Moreo, E. Dagotto, S. Okamoto, S. Kancharla, A. Fujimori, *Phys. Rev. B* **2007**, *76*, 64532.

[2] M. Nakamura, A. Sawa, J. Fujioka, M. Kawasaki, Y. Tokura, *Phys. Rev. B* **2010**, *82*, 201101.

[3] H. Wadati, D. Kobayashi, H. Kumigashira, K. Okazaki, T. Mizokawa, A. Fujimori, K. Horiba, M. Oshima, N. Hamada, M. Lippmaa, *Phys. Rev. B* **2005**, *71*, 035108.

[4] C. Hsu, F. Mansfeld, Corrosion **2001**, 57, 747.